Ion beams in SEM: An experiment towards a high brightness low energy spread electron impact gas ion source

David S. Jun,[a] Vladimir G. Kutchoukov, and Pieter Kruit
Charged Particle Optics Group, Delft University of Technology, Lorentzweg 1, 2628 CJ Delft, The Netherlands

(Received 28 June 2011; accepted 21 October 2011; published 15 November 2011)

A next generation ion source suitable for both high resolution focused ion beam milling and imaging applications is currently being developed. The new ion source relies on a method of which positively charged ions are extracted from a miniaturized gas chamber where neutral gas atoms become ionized by direct electron impact. The use of a very small gas chamber and a very narrow electron beam (<100 nm) allows for a very small ionization volume, which, in turn, yields a small virtual source size and low energy spread. The authors estimate that using a high current density electron beam from a Schottky electron gun the reduced brightness of this source can exceed that of the Gallium Liquid Metal Ion Sources and the energy spread can be well below 1 eV at an optimal gas pressure and gas chamber spacing while producing more than 1 nA of usable ion beam current. In a proof-of-concept study, the authors have produced ions of helium, argon, xenon, and air from a prototype gas chamber using an electron probe inside a scanning electron microscope. Using micro-channel plates and a phosphor screen, ion beam patterns have been acquired demonstrating that a beam of ions can be produced from a miniaturized gas chamber. The authors have measured up to several hundreds of pico-amperes of ion current in a Faraday cup using an input electron probe current of ~14 nA with 1 keV incident energy. The authors have also verified that the ion beam current is dependent on the incident electron beam energy, gas chamber bias voltage, and the gas pressure inside the ionization chamber. © *2011 American Vacuum Society*. [DOI: 10.1116/1.3660390]

I. INTRODUCTION

Focused ion beam (FIB) systems have been indispensible tools in the semiconductor industry, materials science, and many research and applications fields of the nanotechnology sectors because they can image and manipulate nanometer-scaled structures. Similar to scanning electron microscopes (SEMs), FIB systems can provide imaging capability using secondary electron signals from sample but in addition to providing an alternative contrast mechanism using secondary ion signals, the FIB system offers an unparalleled capability of removing materials in the nanometer scale. Some of the key applications of the FIB systems utilizing this unique capability include mask repairs, transmission electron microscope (TEM) sample preparations, integrated circuit (IC) failure analysis, defect characterization, and device modification.[1]

Since the early 1980s, gallium based liquid metal ion sources (Ga LMIS) have been standard for the commercial FIB systems because of their reliable operation with high reduced brightness ($\sim 1 \times 10^6$ A/m^{2}SrV), good current stability ($<\pm 2\%$ on a minute scale), and long life time (~ 400 μA-hours/mg).[1–3] However, the inherent destructive nature of the gallium ions inevitably results in sample destruction making it undesirable for high resolution imaging and inspection applications. Additionally, the Ga LMIS has a relatively high energy spread of 5–10 eV limiting the minimum probe size of the Ga FIB system to be about 10 nm at 30 keV.[1–4] Furthermore, their chemical activity and staining can lead to changes in electrical and magnetic performance, material crystalline change, and chemistry changes in samples.[1]

As the dimensions of the chip components continue to shrink and the demand for more advanced tools to image and manipulate the materials to the atomic scale increases, there has been a growing interest in improving the performance of the FIB systems by developing an ion source with high brightness, low energy spread combined with operation with a broad range of noble ion species and ion currents. Over the course of the past decade, a number of research efforts have emerged to develop noncontaminating FIB source using various methods such as plasma,[5–7] laser photoionization,[8–11] and gas field ionization[12–14] techniques. Unfortunately, some fundamental problems exist in each of these techniques and so far none of these sources is posed to replace the current state-of-the-art Ga LMIS in the commercial FIB systems. Conventional plasma sources have shown to provide reliable production of a variety of noble ion species but their inherent high temperature operation yields a relatively low reduced brightness to compete against the LMIS. Some progress has been achieved in developing a laser ion source using magneto-optical trap (MOT) but researchers are currently facing with a difficulty in achieving high brightness. It is been speculated that the loss in brightness comes from an increase in the transverse temperature of the ion beam from coulomb forces while being extracted from the ionization volume.[9,11] The relatively slow loading rate of the MOT, which eventually limits the extractable current (~160 pA for chromium ion beam[11]) and its complicated aligning and

[a]Author to whom correspondence should be addressed; electronic mail: d.s.jun@tudelft.nl

tuning of laser beams to trap and photo-ionize gas atoms raise some technical and practical concerns. Recently the helium ion microscope based on gas field ionization source (GFIS) from Zeiss has sparked a new interest in ion microscopy. With its light mass and high brightness from gas field ionization, the helium microscope offers exceptional imaging quality but so far the gas species is limited to only helium for reliable operation. With a usable beam current of 1 fA-100 pA of light ions; however, it is inadequate being an effective sputtering tool. The development of a GFIS using a heavier gas such as neon has turned out to be technically difficult due to emission instability and short life time associated with the ionizing gas having a lower ionization energy compared to typical impurities found in the source region.[13,14] The reader is referred to the Ph.D. thesis of Tondare[3] for more in-depth discussions on the recent research efforts in developing a high performance noble gas ion source.

We believe that the next generation ion source for the commercial FIB systems should provide uncompromising performance over all of the fundamental and practical source properties, namely the reduced brightness, energy spread, noise, beam stability, lifetime, and reliability, at least comparable to what the current Ga LMIS offer, while providing a variety of ion species that can be chosen for a specific application without time-consuming modifications (i.e., breaking high vacuum) on the tools. In this paper we introduce a novel concept of an electron impact gas ion source intended to meet all of these requirements and discuss the results of our first experiment toward building such a source.

II. SOURCE CONCEPT

One method to create effective gas ionization is by passing an energetic electron beam through a gas medium. Inelastic collisions between gas atoms and electrons lead to production of ions even at room temperature. This direct electron impact gas ionization is very attractive since room temperature operation warrants for much simpler source integration (without cooling or heating requirement) on the existing commercial FIB systems and also much higher source brightness achievable compared with typical plasma sources.

Figure 1 describes the components and illustrates the concept of our source in its most simplistic view. Essentially, the ion source is comprised of a sub-micron scaled gas chamber and an electron gun. Our preferred electron gun is equipped with a Schottky emitter because along with its reliability, it is known for high brightness that can provide a stable high current (>100 nA) in a small probe size (<100 nm) with proper electron gun optics. The gas chamber can be viewed as a pair of thin parallel conductive membranes separated by a spacing l. The membranes are electrically isolated by a thin layer of an insulator (PMMA, Si_3N_4, SiO_2, etc.). A small bias voltage between the membranes is applied to extract the ions. A pair of small apertures (the double aperture) are created on the stacked membranes by FIB machining so that electrons can enter from one aperture and ions to exit out of the other along with the unscattered electrons. The transmitted electrons are

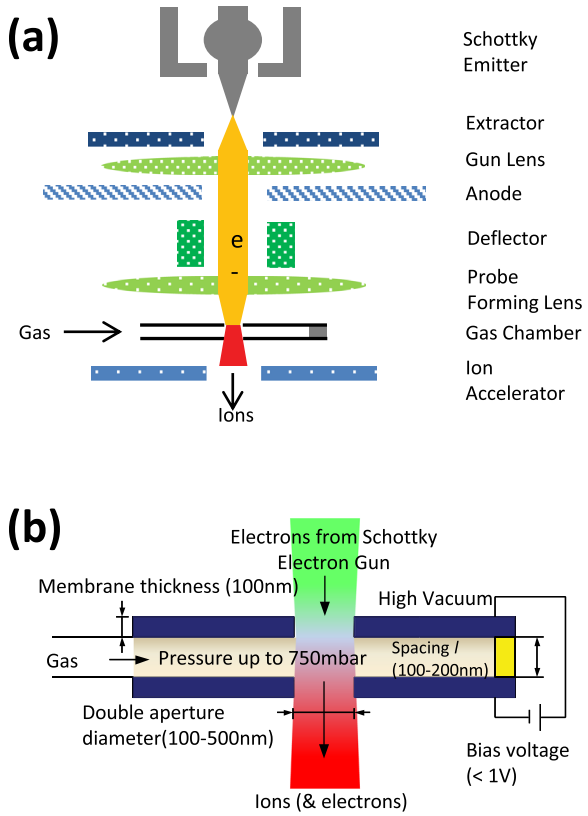

FIG. 1. (Color online) (a) Basic components of our ion source. (b) Target gas chamber dimensions.

repelled while the ions are further accelerated by an ion accelerator placed downstream from the gas chamber. Ideally, the apertures should be kept as small as possible to minimize the neutral gas atoms to escape but also need to be carefully selected to maximize the input electron current and the output ion current.

The miniaturization of the gas chamber is critical because the ionization volume needs to be kept small to provide a small virtual source size thus yielding a high source brightness. Another reason is that in order to minimize the loss in brightness due to ion-ion interactions inside the gas chamber, a high electric field is needed for speedy extraction of the ions, but at the same time, a low bias voltage is preferred in order to keep the ion energy distribution low. To satisfy both conditions, the gas chamber spacing needs to be as small as possible.

III. EXPECTED SOURCE PERFORMANCE

When a number of electrons N_e passes through a gas medium with a uniform particle density n and the partial cross section $\sigma(X)$, under conditions in which very few of the incident electrons produce an ion, N_i the number of X ions produced while the electrons passing through the gas chamber is given by[15]

$$N_i(X) = N_e n l \sigma(X). \quad (1)$$

In order to ensure the extraction of all the ions formed within the length l without collisions with the neutrals, the gas pressure should be maintained such that the mean free path λ of

the neutrals should be longer or at least equal to the gas chamber spacing. For $\lambda = l$, Eq. (1) can be re-written as

$$\frac{N_i(X)}{N_e} = \frac{\sigma(X)}{\sqrt{2}\pi d^2}, \tag{2}$$

where d is the molecular diameter of a given gas atom. Since the ion current is proportional to the number of ions $N_i(X)$ and the electron current the number of electrons N_e the right hand side of Eq. (2) represents the maximum ionization efficiency provided that the gas pressure inside the gas chamber is kept in the molecular flow regime. For argon gas with $d = 0.369$ nm (Ref. 16) and $\sigma(Ar^+) = 0.783 \times 10^{-20}$ m^2 (Ref. 17) for 1 keV incident electron energy, the maximum ion current produced inside the gas chamber is expected to be approximately 1.3% of the input electron current.

It should be noted that we expect the ionization volume to be almost entirely contained inside the gas chamber. A Monte Carlo simulation study by Peatross and Meyerhofer[18] indicates that the gas particle density outside the double aperture is extremely small even for a higher pressure up to $l/\lambda = 10$. Since we intend to run our source in the molecular flow regime, ion-ion collisions and charge transfer outside the gas chamber should be negligible and the source brightness and ion energy distribution should be mainly affected from the ionization inside the gas chamber.

A. Theoretical source brightness

For an ion source emitting a uniform current density J_i at temperature T, the reduced brightness B_r can be estimated by

$$B_r = \frac{eJ_i}{\pi kT}, \tag{3}$$

where e is the electric charge and k is the Boltzmann constant. For our source the ions can only form at the plane of contact with the electron beam area and for a very narrow gas chamber spacing the ion current density is directly proportional to the electron current density but differed by a factor of the right hand side of Eq. (2). In this case, Eq. (3) can be simplified to

$$B_r \approx 2.84 \frac{\sigma(X)J_e}{d^2}, \tag{4}$$

for the reduced brightness unit in A/m^{2}SrV, $T = 293$ K, and the mean free path of the gas atoms matched to the gas chamber spacing ($\lambda = l$).

It is clear from Eq. (4) that for maximizing reduced source brightness it is critical to provide the highest input electron current density as possible. However, because both ionization cross section and the electron current density are dependent on the electron energy, first, a careful examination on the achievable probe current density as a function of beam energy for an electron gun equipped with a Schottky emitter is necessary and thereafter an electron energy that compromises between the ionization cross section and the electron current density to maximize the reduced brightness can be determined.

For minimizing the spot size for a given amount of the probe current, an intricate balancing between the object angle and image angle of an electron gun is necessary under various conditions. In Ref. 19, Kruit *et al*. have provided simple analytical equations to estimate for four different regimes: (1) the chromatic aberration Cc of the probe lens dominates a system, (2) the spherical aberration Cs of the probe lens dominates, (3) the brightness does not play role but the chromatic aberration of the gun lens needs to be balanced with the chromatic aberration of the probe lens, and (4) the spherical aberration of the gun lens needs to be balanced with the spherical aberration of the probe lens. Following the steps provided in Ref. 19, the possible current density of a gun with a Schottky emitter for the electron acceleration voltages of 100 to 1000 V are calculated and presented in Fig. 2. The input parameter values used for the calculation such as reduced brightness, virtual source size, angular intensity, and energy spread for typical Schottky sources and the aberration coefficients of typical gun lens are taken from Ref. 20. For the aberration coefficients Cs and Cc of the probe forming lens we have used more conservative values of 0.3 mm for 100 V and 1 mm for 1000 V and varying linearly with the acceleration voltage for the voltages in between.

Figure 3 shows the estimated reduced source brightness as a function of the incident electron energy for singly charged ion beams of helium, neon, argon, krypton, and xenon. The values are calculated using Eq. (4) with the electron current densities from Fig. 2 and the partial ionization cross sections of those gases found in Ref. 17. The results indicate that the reduced source brightness of our source can be more than an order of magnitude higher than the Ga LMIS. Note that the maximum reduced brightness arises with an incident electron energy around 300–500 eV although the ionization cross sections of these gases typically peak around 50 eV.

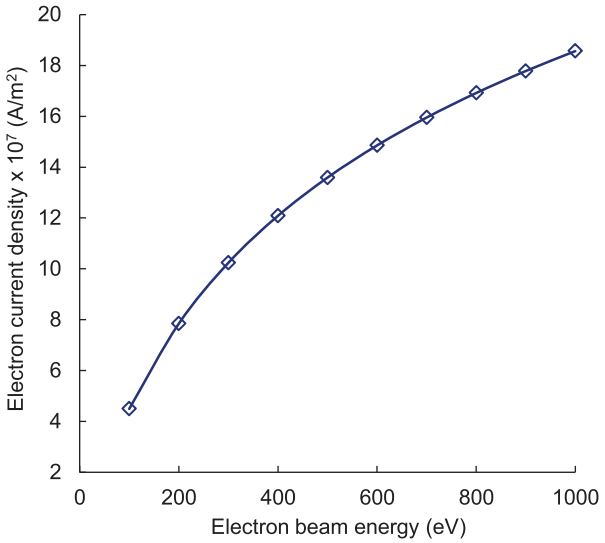

FIG. 2. (Color online) Electron current density as a function of beam energy for an electron gun equipped with a Schottky source.

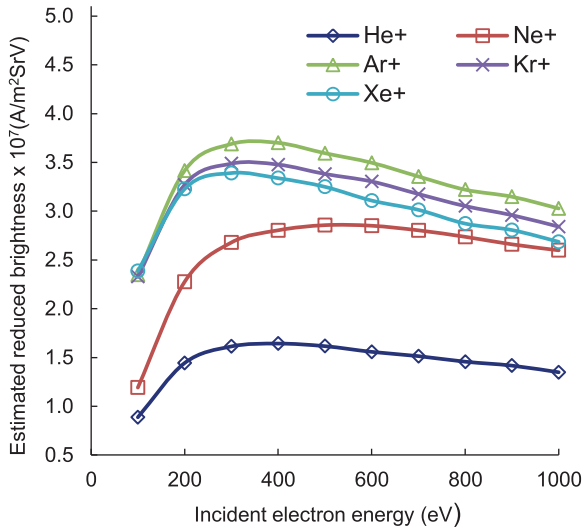

FIG. 3. (Color online) Estimated reduced source brightness for helium, neon, argon, krypton, and xenon ions.

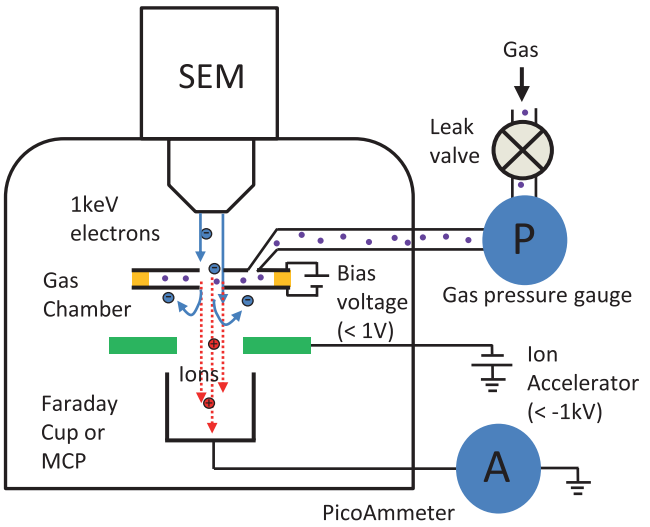

FIG. 4. (Color online) Schematic representation of the experimental test setup.

B. Ion energy distribution

For the new ion source it is preferred to have a large extraction field inside the gas chamber to reduce the ion flight time so that the probability of charge transfer and coulomb interactions caused by ion-ion collisions decreases. One attractive feature about the miniaturized gas chamber design is that even a small bias voltage can generate a relatively large field inside the gas chamber. For a spacing of 100 nm, only 0.3 V is necessary to create an e-field of $\sim 3 \times 10^6$ V/m, which is a moderate field below the threshold for field-induced breakdown over the insulating medium between the membranes. The argon ion flight time across the 100 nm spacing in such field is approximately 0.083×10^{-9} sec implying that only one ion at a time can form and exit the gas chamber for an ion current up to almost 2 nA. Under these circumstances, ion-ion coulomb interaction inside the gas chamber becomes negligible and the energy distribution should only depend on the angular spread set by the initial thermal motion of the ions at the time of ionization and the spatial distribution of the ions along the beam axis within the extraction field inside the gas chamber. Judging from the fact that the average thermal energy of gas particles at room temperature (~0.04 eV for argon) is much lower than the energy of a typical ion gained by the bias voltage (0.3 V for 100 nm spacing), it is anticipated that the energy distribution of our source is mostly governed by the gas chamber bias voltage.

IV. PROOF-OF-CONCEPT EXPERIMENT

A. Experimental setup

A proof-of-concept experiment with the goals of testing our gas chamber membranes for its mechanical integrity under a gas load and demonstrating the idea of generating and extracting an ion beam from a prototype gas chamber has been conducted in a FEI Quanta 3D FEG Dual Beam (we refer this tool as simply "SEM" in this paper for convenience). The SEM is perfect for our purposes as its specimen chamber can be used as a simple vacuum testing space with the convenience of quick venting and pump-down and many extra ports are available for customizing a gas delivery system and electrical connections, and most importantly, a wide range of electron beam currents even at low accelerating voltages (up to 24 nA at 1 keV) are easily accessible for attempting direct electron impact ionization inside our prototype gas chambers.

Figure 4 shows a simple schematic of our apparatus. The test setup consists of two main sections—gas chamber housing and a changeable detection system, a Faraday cup or a combination of microchannel plates (MCP) and a phosphor screen. The gas chamber housing holds a prototype chamber (Figs. 5 and 6) and a gas tubing that originated from a gas bottle outside of the SEM chamber. An O-ring is used to make a leak tight connection between the gas feed window of the gas chamber and the gas tubing. The gas chamber housing also holds the ion accelerator, which is used to repel the transmitted electrons and accelerate the ions towards the detection system. For imaging an ion beam pattern, ion signals are first converted to amplified electron signals by MCP and the electron signals are then projected on a phosphor screen. For measuring an ion beam current, a Faraday cup is mounted below the gas chamber housing and connected to a current meter.

The entire test setup including the detection system is mounted on the SEM sample stage. At the beginning of the experiment, the setup is first roughly aligned to the electron column by stage movement. The gas chamber is imaged by the SEM, the double aperture located, and then a precise alignment of the electron probe and the center of the gas chamber double aperture made. The electron beam can be kept scanning over the double aperture to supply a pulsed electron beam into the gas chamber or can be switched to spot mode to supply a steady electron beam into the gas chamber. The gas load to the gas chamber is controlled by a manual leak valve outside the SEM chamber. A vacuum

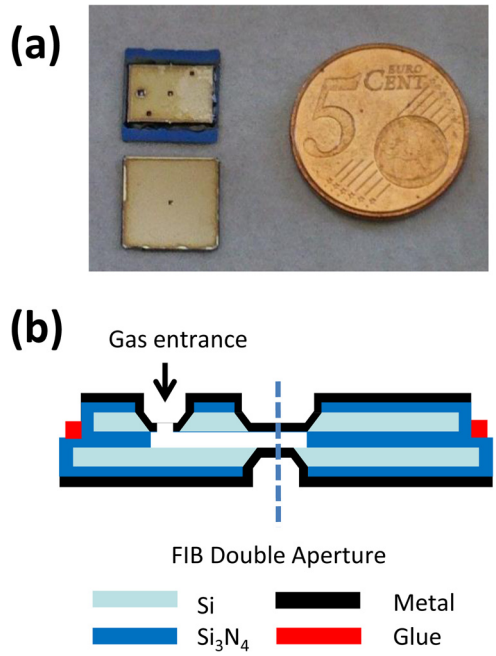

FIG. 5. (Color online) (a) Top and bottom view of a prototype gas chamber. (b) Gas chamber cross section. The gas chamber is a glued structure of two silicon substrates (~700 μm total thickness). On each substrate a 100 nm thick molybdenum membrane is prepared through several steps of metal evaporation, e-beam lithography, and wet-etching. A gas channel is dry-etched on the Si_3N_4 layer on each substrate. After the membranes are aligned and the substrates glued together, a double aperture is FIB-milled to create electron/ion entrance/exit holes.

pressure gauge suitable for all gas types (DCP 3000, Vacuubrand) is placed near the leak valve to monitor the amount of gas being leaked in to the gas chamber.

B. Results

Each prototype gas chamber is first inspected by SEM imaging to measure the double aperture diameter and the gas chamber spacing. The gas chamber spacing can be back-calculated from measuring the change in the amount of the lower aperture edge showing through the upper aperture when the gas chamber is tilted by a certain amount (Fig. 6). With our current gas chamber fabrication process, our typical gas chamber spacing is 1–2 μm although the fabrication method is designed for 100–200 nm spacing. Our analysis indicates that particle contaminations and glue seepage are

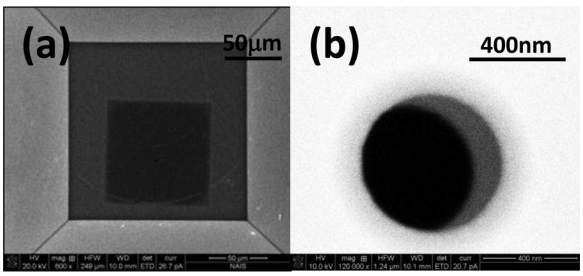

FIG. 6. SEM micrographs of a prototype gas chamber. (a) Small membrane (~80 × 80 μm) showing through the larger membrane (~150 × 150 μm). (b) A tilted view of a FIB-milled double aperture. The tilted view clearly shows a small separation between the two membranes.

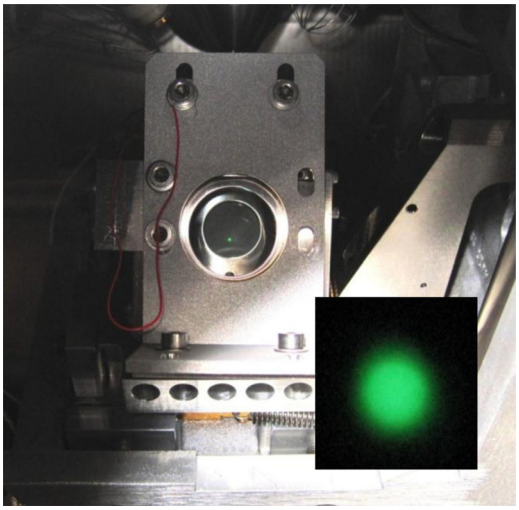

FIG. 7. (Color online) Ion beam pattern imaging setup and an argon ion beam pattern projected on the phosphor screen (inset).

responsible for the increased spacing. We are currently working to improve our process control and gluing process as well as exploring for glue-less alternatives such as wafer bonding and surface micromachining techniques.

An example of argon ion beam pattern we observed is shown in Fig. 7. The intensity of the beam pattern strongly depends on the gas chamber pressure and a slight change in the beam size is noted when the ion accelerator bias was changed. When the electron beam is scanned over the double aperture, a pulsed ion beam signal is also observed on the phosphor screen. All these observations prove that the ions extracted from our miniaturized gas chamber are indeed in a form of beam.

Figure 8 shows the extracted ion current as a function of the gas pressure for helium, argon, xenon, and air. The results clearly indicate that the amount of ions generated from the gas chamber depends on the type of ionizing gas

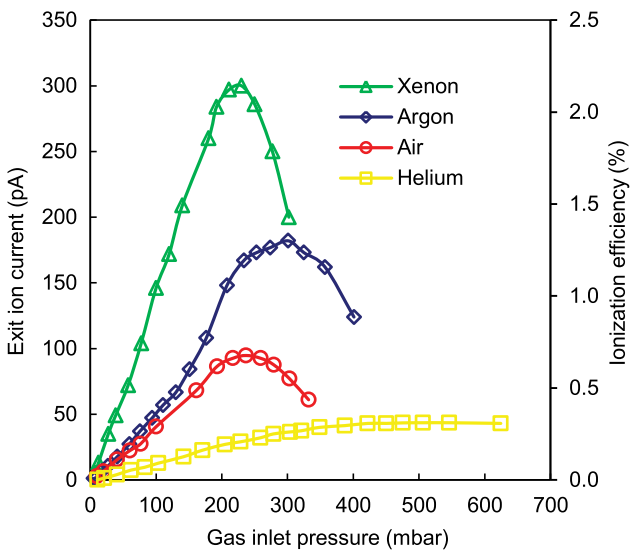

FIG. 8. (Color online) Measured ion current for argon, helium, xenon, and air with an input electron probe current of ~14 nA with 1 keV energy (gas chamber spacing = 2.3 μm, aperture diameter = 1.5 μm).

and the gas pressure. The differences in the measured ion currents among the gases reflect the fact that each gas has a different electron impact ionization cross section for a given incident electron beam energy. The figure also clearly shows deteriorating ion current at higher pressures indicating ion transmission rate dependence on the mean free path of gas particles inside the gas chamber. One thing to note is that we expect that the actual pressure inside the gas chamber is very close to what the inlet pressure gauge near the leak valve measures as we have observed only a very small pressure change in the SEM chamber even a high gas load is applied in the gas chamber. We can maintain a SEM chamber pressure in the 10^{-6} mbar range (the base pressure of the SEM chamber without any gas load in the gas chamber is in the low 10^{-6} mbar) even with almost an atmospheric gas pressure (measured at the inlet pressure gauge) is leaked into the gas chamber. Another observation is that when the gas leak valve is closed, the pressure reading of the inlet gas pressure gauge drops very slowly ($< 1\%$/hour) meaning very little gas is lost through the double aperture.

As expected, the amount of ion current extracted from our gas chambers strongly depends also on the incident electron beam energy. Figure 9 shows the measured ionization efficiency (extracted ion current/input electron current) as a function of the incident electron beam energies between 800 and 1500 V. The trend seen in the measurement is in good agreement with published ionization cross sections.

The gas chamber bias voltage is another factor that regulates the amount of extracted ion current (Fig. 10). The angular spread set by the initial thermal motion of the ions at the time of ionization and the e-field between the two membranes determine the transmission of ions through the ion exit aperture. As expected, the extracted ion current increases with the gas chamber bias voltage until the ion beam size becomes smaller than the aperture size. It is interesting that even with a zero bias voltage; still some amount of extracted ion current is seen. This is explained by the e-field created by the ion accelerator still leaking in to the gas chamber.

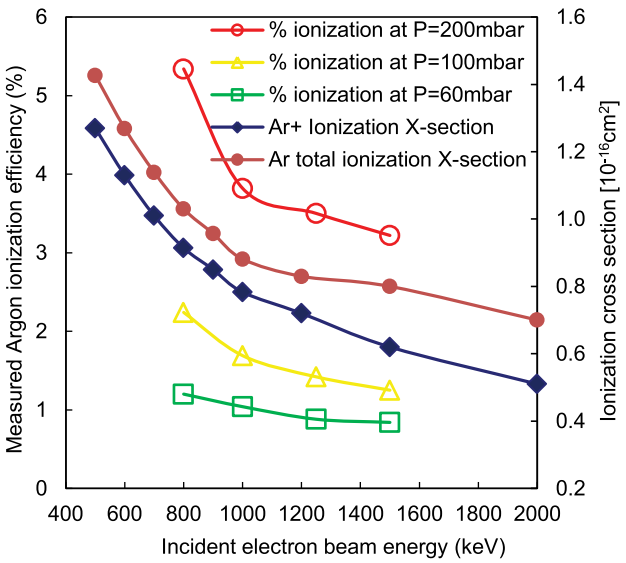

FIG. 9. (Color online) Ion current as a function of the incident electron energy (gas chamber spacing = 1.4 mm, aperture diameter = 1 mm). The Ar^+/Ar total ionization cross sections cited from Refs. 17 and 21.

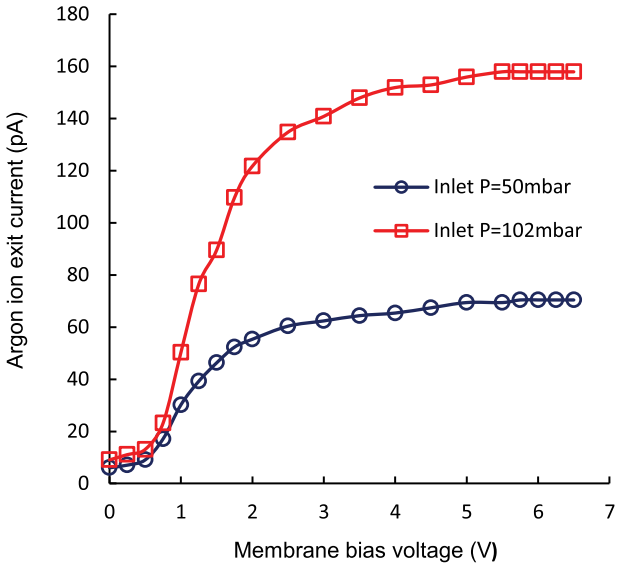

FIG. 10. (Color online) Gas chamber membrane bias voltage effect. A higher bias voltage can squeeze more ions into the ion exit aperture (gas chamber spacing = 1.4 μm, aperture diameter = 1 μm, SEM probe current ~9 nA).

V. CONCLUSIONS

We are working towards designing and constructing a high brightness, low energy spread gas ion source based on direct electron impact ionization. The aim of our research is to develop a noncontaminating FIB source that's suitable for both high resolution imaging and milling applications. In this paper, we have presented the concept of our source as well as the results of our proof-of-concept experiments. We have acquired ion beam patterns and demonstrated that it is possible to generate a variety of noble species ion beams from a miniaturized gas chamber. We have verified that the amount of the ion current extracted from such a gas chamber greatly depends on the gas chamber pressure, incident electron beam energy, and gas chamber bias voltage. We plan to improve our gas chamber spacing and measure the energy spread and brightness of our source in the near future.

ACKNOWLEDGMENTS

This research is supported by the "Stichting voor Fundamenteel Onderzoek der Materie (FOM)," which is financially supported by the "Nederlandse Organisatie voor Wetenschppelijk Onderzoek" and FEI Company.

[1]M. Utlaut, *Handbook of Charged Particle Optics*, 1st ed., edited by J. Orloff (CRC, New York, 1997), Chap. 11.
[2]L. A. Giannuzzi and F. A. Stevie, *Introduction to Focused Ion Beams: Instrumentation, Theory, Techniques and Practice* (Springer, New York, 2005).
[3]V. N. Tondare, "Towards a high brightness, monochromatic electron impact gas ion source," Ph.D. dissertation (Delft University of Technology, 2006).
[4]J. Gierak, A. Septier, and C. Vieu, Nucl. Instrum. Methods Phys. Res. A **427**, 91 (1999).
[5]L. Scipioni, D. Stewart, D. Ferranti, and A. Saxonis, J. Vac. Sci. Technol. B **18**, 3194 (2000).

[6]Q. Ji, T.-J. King, K.-N. Leung, and S. B. Wilde, Rev. Sci. Instrum. **73**, 822 (2002).
[7]N. S. Smith, P. P. Tesch, N. P. Martin, and R. W. Boswell, *Microscopy Today* (Cambridge University, Cambridge, 2009), Vol. 17, pp. 18–23.
[8]J. L. Hanssen, E. A. Dakin, J. J. McClelland, and M. Jacka, J. Vac. Sci. Technol. B **24**, 2907 (2006).
[9]S. B. van der Geer, M. P. Reijnders, M. J. de Loos, E. J. D. Vredenbregt, P. H. A. Mutsaers, and O. J. Luiten, J. Appl. Phys. **102**, 094312 (2007).
[10]B. J. Claessens, M. P. Reijnders, G. Taban, O. J. Luiten, and E. J. D. Vredenbregt, Phys. Plasmas **14**, 093101 (2007).
[11]A. V. Steele, B. Knuffman, J. J. McClelland, and J. Orloff, J. Vac. Sci. Technol. B **28**, C6F1 (2010)
[12]J. Notte, R. Hill, S. McVey, L. Farkas, R. Percival, B. Ward, Microsc. Microanal. **12**, 126 (2006).
[13]J. Notte, F. H. M. Rahman, S. M. McVey, S. Tan, and R. Livengood, Microsc. Microanal. **16**, 28 (2010).
[14]R. H. Livengood, S. Tan, R. Hallstein, J. Notte, S. McVey, F. H. M. Rahman, Nucl. Instrum. Methods Phys. Res. A **645**, 136, (2011).
[15]H. C. Straub, P. Renault, B. G. Lindsay, K. A. Smith, and R. F. Stebbings, Phys. Rev. A **52**,115 (1995).
[16]A. Roth, *Vacuum Technology*, 2nd. ed. (Elsevier, New York, 1990).
[17]R. Rejoub, B. G. Lindsay, and R. F. Stebbings, Phys. Rev. A **65**, 042713 (2002).
[18]J. Peatross and D. D. Meyerhofer, Rev. Sci. Instrum. **64**(11), 3066 (1993).
[19]P. Kruit, M. Bezuijen, and J. E. Barth, J. Appl. Phys. **99**, 024315 (2006).
[20]L. W. Swanson and G. A. Schwind, *Handbook of Charged Particle Optics*, 1st ed., edited by J. Orloff (CRC, New York, 1997), Chap. 2.
[21]P. L. Bartlett and A. T. Stelbovics, Phys. Rev. A **66**, 012707 (2002).